CCFE
CULHAM CENTRE FOR FUSION ENERGY

UK Atomic Energy Authority

UKAEA-CCFE-PR(19)53

S. Buller, A. Mollen, S.L. Newton, H.M. Smith, I. Pusztai

The importance of the classical channel in the impurity transport of optimized stellarators

The importance of the classical channel in the impurity transport of optimized stellarators

S. Buller, A. Mollén, S.L. Newton, H.M. Smith, I. Pusztai

This is a preprint of a paper submitted for publication in
Journal of Plasma Physics

The importance of the classical channel in the impurity transport of optimized stellarators

S. Buller, A. Mollén, S.L. Newton, H.M. Smith, I. Pusztai

(Received xx; revised xx; accepted xx)

In toroidal magnetic confinement devices, such as tokamaks and stellarators, neoclassical transport is usually an order of magnitude larger than its classical counterpart. However, when a high-collisionality species is present in an stellarator optimized for low Pfirsch-Schlüter current, its classical transport can be comparable to the neoclassical transport. In this letter, we compare neoclassical and classical fluxes and transport coefficients calculated for W7-X and Large Helical Device (LHD) cases. In W7-X, we find that the classical transport of a collisional impurity is comparable to the neoclassical transport for all radii. Even for the LHD case – which has not been optimized for low Pfirsch-Schlüter current – the classical transport can still be comparable to the neoclassical at specific radii.

The most developed concepts for achieving controlled thermonuclear fusion are the tokamak and stellarator. Both the tokamak and the stellarator utilize a strong toroidal magnetic field to confine a hot plasma in which fusion reactions take place.

When such a plasma is in a steady-state, loss of particles and energy mainly occurs as a result of micro-turbulence, collisions, or direct losses of particles on unconfined orbits. The two latter processes – and the resulting transport of particles and heat – is referred to as *collisional transport*, and can be modeled within the framework of drift-kinetics. Historically this is the dominant transport channel in the core of stellarators due to large direct losses from unconfined orbits (Beidler *et al.* 2012).

Collisional transport can be further separated into two additive components: classical transport, which is due to the gyro-motion of particles around the magnetic field-lines, and neoclassical transport, which is due to the complex orbits carried out by the center of gyration as it moves in the magnetic field. The latter typically leads to much larger transport than the former (Pfirsch & Schlüter 1962), and also accounts for the large direct losses in stellarators, with a very strong unfavorable scaling towards reactor-relevant high temperatures. Thus, much effort has been devoted to reducing the neoclassical transport in stellarators, resulting in optimized stellarators such as Wendelstein 7-X (W7-X) (Nührenberg & Zille 1986), while classical transport is often neglected.

However, it has not been widely appreciated that, as a result of optimizing for low neoclassical transport and Pfirsch-Schlüter current, the neoclassical transport of impurities in W7-X can now be comparable to the often neglected classical transport. The main purpose of the present note is to raise attention to this circumstance.

To understand why the classical transport is relevant in an optimized stellarator, we employ recent analytical results on neoclassical transport for a collisional impurity(Braun & Helander 2010; Helander *et al.* 2017; Newton *et al.* 2017) to show that the ratio of classical to neoclassical fluxes is proportional to a geometrical factor (1.1), which turns out to be larger than one in W7-X.

Motivated by these results, we present a general expression for the classical transport,

using the linearized Fokker-Planck operator and allowing for an arbitrary number of species. The employed collision operator is frequently used in modern neoclassical solvers, and the results can thus be directly compared with the output from such codes. In the final section, we look at a few example magnetic configurations, where compare the magnitude of the classical transport to that of the neoclassical transport calculated with the SFINCS† drift-kinetic solver (Landreman *et al.* 2014), and investigate the collisionality dependence of the ratio of neoclassical to classical transport.

1. Motivation

Before performing a detailed analysis, it is useful to consider a simple (but experimentally relevant) limit, where the importance of classical transport in a stellarator is apparent. For this purpose, we summarize results from earlier work (Buller *et al.* 2018; Braun & Helander 2010; Helander *et al.* 2017).

At fusion-relevant temperatures, the bulk hydrogen species of the confined plasma will be in a low-collisionality regime. However, as the collisionality increases with charge, high-Z impurities (with Z being the charge number) can still have high collisionality. Such impurities can occur, for example, in experiments using tungsten plasma-facing component, which is the favoured material for the divertor of future fusion reactors (Bolt *et al.* 2002). These plasmas will thus be in a *mixed-collisionality regime*, with low-collisionality bulk and high-collisionality impurity ions.

In this regime, the ratio of classical to neoclassical impurity particle fluxes calculated from the mass-ratio expanded collision operator is given by a purely geometrical factor (Buller *et al.* 2018)

$$\frac{\langle \boldsymbol{\Gamma}_z \cdot \nabla\psi \rangle^{\mathrm{C}}}{\langle \boldsymbol{\Gamma}_z \cdot \nabla\psi \rangle^{\mathrm{NC}}} = \frac{\langle j_\perp^2 \rangle \langle B^2 \rangle}{\left\langle j_\parallel^2 \right\rangle \langle B^2 \rangle - \langle j_\parallel B \rangle^2}. \tag{1.1}$$

Here, ψ is a radial coordinate (a flux surface label), $\langle\cdot\rangle$ is the flux-surface average, $\boldsymbol{\Gamma}_z$ is the flux of impurity ions, $\langle \boldsymbol{\Gamma}_z \cdot \nabla\psi \rangle^{(\mathrm{N})\mathrm{C}}$ is the radial (neo)classical impurity flux averaged over the flux-surface, $\boldsymbol{B}$ is the magnetic field, $B = |\boldsymbol{B}|$, and $\boldsymbol{j}$ is the current density, here defined by $\boldsymbol{B} \times \boldsymbol{j} = \nabla p(\psi)$, $\nabla \cdot \boldsymbol{j} = 0$; with $j_\parallel$ and $j_\perp$ being the current components parallel and perpendicular to $\boldsymbol{B}$, and p the total pressure.

Equation 1.1 also enters into the ratio of classical and neoclassical transport at yet higher collisionalities: in the Pfirsch-Schlüter regime, where both bulk and impurity ions are collisional, which is readily shown using the expression for neoclassical transport derived by Braun & Helander (2010) together with the expression for classical transport derived by Buller *et al.* (2018). For stellarators optimized for low $j_\parallel/j_\perp$ (such as W7-X), the (1.1) ratio will be large and classical transport will thus dominate at high collisionality. This will be verified by numerical simulations in Sec. 3.

2. Linearized Fokker-Planck operator

In this section, we write down the classical particle and heat transport due to a linearized Fokker-Planck operator. The flux-surface averaged radial classical transport

† Available at: `https://github.com/landreman/sfincs` (verified 2019-01-28)

is given by

$$\Gamma_a^{\mathrm{C}} \equiv \langle \boldsymbol{\Gamma}_a \cdot \nabla\psi \rangle^{\mathrm{C}} \equiv \left\langle \frac{\boldsymbol{b}\times\nabla\psi}{Z_a e B} \cdot \boldsymbol{R}_a \right\rangle, \tag{2.1}$$

$$Q_a^{\mathrm{C}} \equiv \langle \boldsymbol{Q}_a \cdot \nabla\psi \rangle^{\mathrm{C}} \equiv \left\langle \frac{\boldsymbol{b}\times\nabla\psi}{Z_a e B} \cdot \boldsymbol{G}_a \right\rangle, \tag{2.2}$$

where we have introduced the *friction force* and *energy-weighted friction force*

$$\boldsymbol{R}_a \equiv \int \mathrm{d}^3 v m_a \boldsymbol{v} C[f_a], \tag{2.3}$$

$$\boldsymbol{G}_a \equiv \int \mathrm{d}^3 v \frac{m_a v^2}{2} m_a \boldsymbol{v} C[f_a]. \tag{2.4}$$

Here, $C[f_a] = \sum_b C_{ab}[f_a, f_b]$ is the Fokker-Planck collision operator, accounting for the collisions of all species 'b' with species 'a'; f_a the distribution function of species 'a', with mass m_a and charge $Z_a e$, with e the elementary charge; the integral is over all velocities $\boldsymbol{v}$. In a confined plasma, the distribution functions are close to a Maxwell-Boltzmann distribution f_{a0}, such that $f_a = f_{a0} + f_{a1}$, and f_{a1} satisfies $f_{a1}/f_{a0} \ll 1$. For later reference, we also define the classical conductive heat flux $q_a^{\mathrm{C}} = Q_a^{\mathrm{C}} - \frac{5}{2} T_a \Gamma_a^{\mathrm{C}}$, where T_a is the temperature of species 'a'.

For a magnetized plasma, it is useful to separate out the dependence of the distribution function on the gyrophase. Only the gyrophase-dependent part of f, which we denote by $\tilde{f}$, contributes to $\boldsymbol{R}$ and $\boldsymbol{G}$ perpendicular to the magnetic field, and thus to the classical fluxes (2.1)-(2.2). For a magnetized plasma with an isotropic Maxwellian, it is well-known that (Hazeltine 1973)

$$\tilde{f}_{a1} = -\boldsymbol{\rho}_a \cdot \nabla f_{a0}, \tag{2.5}$$

where $\boldsymbol{\rho}_a = \boldsymbol{B} \times \boldsymbol{v} m_a / (Z_a e B^2)$ is the gyro-radius vector.

With (2.5), we can readily evaluate the classical transport given by (2.1)-(2.4). Lately in stellarator research, the importance of flux-surface variation of the electrostatic potential has been recognized (García-Regaña *et al.* 2017); such effects can be incorporated into the classical transport by including the flux-surface varying part of the potential in the Maxwell-Boltzmann distribution f_0 (Hinton & Wong 1985)

$$f_0 = \eta(\psi) \left(\frac{m}{2\pi T}\right)^{3/2} \exp\left(-\frac{m v^2}{2T} - \frac{Ze\tilde{\Phi}}{T}\right), \tag{2.6}$$

where Φ is the electrostatic potential, $\tilde{\Phi} = \Phi - \langle \Phi \rangle$, and we have introduced the *pseudo-density*

$$\eta(\psi) \equiv n \mathrm{e}^{\frac{Ze\tilde{\Phi}}{T}}, \tag{2.7}$$

with n the density. In terms of gradients of η, T and Φ, the gradient in (2.5) thus becomes,

$$\nabla f_0 = \nabla\psi \frac{\partial f_0}{\partial \psi} = \nabla\psi f_0 \left[\frac{\mathrm{d}\ln\eta}{\mathrm{d}\psi} + \frac{Z_a e}{T_a}\frac{\partial\tilde{\Phi}}{\partial\psi} + \frac{Z_a e\tilde{\Phi}}{T_a}\frac{\mathrm{d}\ln T_a}{\mathrm{d}\psi} + \left(\frac{m_a v^2}{2T_a} - \frac{3}{2}\right)\frac{\mathrm{d}\ln T_a}{\mathrm{d}\psi} \right]. \tag{2.8}$$

With this f_0, the resulting classical fluxes can be calculated analogously to Ref. (New-

ton & Helander 2006), resulting in

$$\begin{aligned}\Gamma_a = \frac{m_a}{Z_a e^2}\sum_b \frac{1}{\tau_{ab} n_b}\Bigg[&\left\langle n_a n_b \frac{|\nabla\psi|^2}{B^2}\right\rangle M_{ab}^{00}\left(\frac{T_a}{Z_a}\frac{\mathrm{d}\ln\eta_a}{\mathrm{d}\psi} - \frac{T_b}{Z_b}\frac{\mathrm{d}\ln\eta_b}{\mathrm{d}\psi}\right)\\ &+\left\langle n_a n_b \frac{|\nabla\psi|^2}{B^2} e\tilde{\Phi}\right\rangle M_{ab}^{00}\left(\frac{\mathrm{d}\ln T_a}{\mathrm{d}\psi} - \frac{\mathrm{d}\ln T_b}{\mathrm{d}\psi}\right)\\ &+\left\langle n_a n_b \frac{|\nabla\psi|^2}{B^2}\right\rangle \Bigg(\left(M_{ab}^{00} - M_{ab}^{01}\right)\frac{T_a}{Z_a}\frac{\mathrm{d}\ln T_a}{\mathrm{d}\psi}\\ &\qquad - \left(M_{ab}^{00} - \frac{m_a T_b}{m_b T_a} M_{ab}^{01}\right)\frac{T_b}{Z_b}\frac{\mathrm{d}\ln T_b}{\mathrm{d}\psi}\Bigg)\Bigg],\end{aligned} \tag{2.9}$$

$$\begin{aligned}q_a = -\frac{T_a m_a}{Z_a e^2}\sum_b \frac{1}{\tau_{ab} n_b}\Bigg[&\left\langle n_a n_b \frac{|\nabla\psi|^2}{B^2}\right\rangle M_{ab}^{01}\left(\frac{T_a}{Z_a}\frac{\mathrm{d}\ln\eta_a}{\mathrm{d}\psi} - \frac{T_b}{Z_b}\frac{\mathrm{d}\ln\eta_b}{\mathrm{d}\psi}\right)\\ &+\left\langle n_a n_b \frac{|\nabla\psi|^2}{B^2} e\tilde{\Phi}\right\rangle M_{ab}^{01}\left(\frac{\mathrm{d}\ln T_a}{\mathrm{d}\psi} - \frac{\mathrm{d}\ln T_b}{\mathrm{d}\psi}\right)\\ &+\left\langle n_a n_b \frac{|\nabla\psi|^2}{B^2}\right\rangle \Bigg(\left(M_{ab}^{01} - M_{ab}^{11}\right)\frac{T_a}{Z_a}\frac{\mathrm{d}\ln T_a}{\mathrm{d}\psi}\\ &\qquad - \left(M_{ab}^{01} + N_{ab}^{11}\right)\frac{T_b}{Z_b}\frac{\mathrm{d}\ln T_b}{\mathrm{d}\psi}\Bigg)\Bigg],\end{aligned} \tag{2.10}$$

where M_{ab}^{jk} are the Braginskii matrix elements (Braginskii 1958), defined in Appendix A, using the same notation as Helander & Sigmar (2005); the collision time τ_{ab} is defined as

$$\frac{1}{\tau_{ab} n_b} \equiv \frac{\sqrt{2} Z_a^2 Z_b^2 e^4 \ln\Lambda}{12\pi^{3/2}\epsilon_0^2 m_a^{1/2} T_a^{3/2}}, \tag{2.11}$$

where $\ln\Lambda$ the Coulomb logarithm, and ϵ_0 the vacuum permittivity. These expressions are valid for all collisionalities. In (2.9) and (2.10), the effect of $\tilde{\Phi}$ is to induce a weighting over the flux-surface due to the flux-surface variation of n_a and its radial gradient. Note that the radial electric field (from $\langle\Phi\rangle$ and $\tilde{\Phi}$) does not contribute in the above expression, even when $\frac{\mathrm{d}\ln\eta}{\mathrm{d}\psi}$ is expressed in terms of (2.7).

In (2.9) – (2.10), the $|\nabla\psi|^2$ factors corresponds to the $j_\perp$ factor in (1.1), while the $j_\parallel$ factor in (1.1) arises due to the neoclassical transport (Braun & Helander 2010; Helander *et al.* 2017). In the following section, we will evaluate the above expression for example magnetic configurations.

3. Comparison to neoclassical calculations

In this section, the classical fluxes in (2.9) and (2.10) will be compared to the neoclassical fluxes calculated by the drift-kinetic solver SFINCS, which has the option to use the same collision operator and definition of f_0. This allows us to assess the relative importance of classical and neoclassical particle transport of any species across collisionality regimes.

As indicated at the end of Sec. 1, we expect classical transport to dominate at high collisionality in a stellarator optimized for low parallel current. To study the transition to the high-collisionality asymptotes in more detail, we artificially change the collisionality at a flux-surface ($r_N = 0.88$, where $r_N = \sqrt{\psi_\mathrm{t}/\psi_{\mathrm{t,LCFS}}}$, with ψ_t the toroidal flux and $\psi_{\mathrm{t,LCFS}}$ its value at the last-closed flux-surface) in a W7-X standard configuration, studied by Mollén *et al.* (2015), and a Large Helical Device (LHD) impurity hole discharge

(#113208, $t = 4.64\,\mathrm{s}$, at $r_N = 0.6$), studied by Mollén *et al.* (2018). To make the scan computationally feasible, effects of $\tilde{\Phi}$ and the radial electric field are not included (the radial electric field is set to $10^{-3} \approx 0$ in the simulations). Both effects can reduce or enhance the neoclassical transport, but do not affect the classical transport strongly. As $\tilde{\Phi} = 0$, the density is a flux-function, and $\eta_a = n_a$.

For each point in the collisionality scan, we calculate the neoclassical and classical transport coefficients of the hydrogen bulk ion and a carbon impurity. The transport coefficients for the (neo)classical fluxes are defined such that

$$\Gamma_a^{(\mathrm{N})\mathrm{C}} = -n_a \left(D_{a,ni}^{(\mathrm{N})\mathrm{C}} \frac{\mathrm{d}\ln n_i}{\mathrm{d}\psi} + D_{a,nz}^{(\mathrm{N})\mathrm{C}} \frac{\mathrm{d}\ln n_z}{\mathrm{d}\psi} + D_{a,T}^{(\mathrm{N})\mathrm{C}} \frac{\mathrm{d}\ln T}{\mathrm{d}\psi} \right), \tag{3.1}$$

where $a = i, z$ for ions and impurities, and we have neglected the effects of electron collisions on the ion fluxes due to the small electron-to-ion mass-ratio, and assumed that the ions have the same temperature $T \equiv T_i = T_z$.

The results of the collisionality scan are shown in Fig. 1, with the collisionality defined as

$$\hat{\nu}_{ab} = \frac{G + \iota I}{B_0 \sqrt{2T_a/m_a}} \frac{1}{\tau_{ab}}. \tag{3.2}$$

As seen in the left panels of Fig. 1, the impurity transport coefficients in the W7-X geometry are dominantly classical already for $\hat{\nu}_{CC} \gtrsim 1$, and the cross-species contributions are classically-dominated already for $\hat{\nu}_{CC} \gtrsim 0.1$, for both the bulk and the impurity ions. On the other hand, in LHD – which has not been optimized for low $|j_\parallel|/|\boldsymbol{j}_\perp|$ – the classical transport is at least an order of magnitude smaller than the neoclassical transport for both species at the same collisionalities, and only becomes comparable to the neoclassical at collisionalities approximately 10 times higher.

4. Discussion

We have seen that the neoclassical and classical transport coefficients can become comparable in W7-X even at modest impurity collisionality ($\hat{\nu}_{\mathrm{CC}} \gtrsim 0.1 - 1$), although these simulations do not include effects of electrostatic potential variation on the flux-surface, collisions with electrons or the effects of a radial electric field. To assess the relative importance of neoclassical and classical transport in realistic scenarios with these effects included, we consider two cases in which the full neoclassical behaviour has been analyzed by Mollén *et al.* (2018): a high-mirror W7-X scenario, and the LHD case of the previous section with an additional helium impurity. The results are shown in Fig. 2 (left panels, W7X; right panels, LHD). We note that in the W7-X case, the classical to neoclassical neon flux ratio is around 0.5 in magnitude at most radii, and is not very sensitive to the effects of $\tilde{\Phi}$.

In the LHD case, the classical to neoclassical flux ratio for helium is mostly in the range of 10^{-2}, while it is order unity in the deep core ($r_N \approx 0.2$). The flux ratio for carbon reaches unity values at several radial locations ($r_N \leqslant 0.3$ and $0.6 \lesssim r_N \lesssim 0.8$). For outer radii, $\tilde{\Phi}$ has a very large effect on the carbon fluxes: when $\tilde{\Phi}$ is set to zero, the neoclassical carbon flux becomes 40 times smaller than the classical flux in the region $r_N \in [0.6, 0.8]$. This region coincides with a region of carbon collisionalities in the range of $[0.07, 0.4]$ – which is where the neoclassical $D_{C,ni}$ coefficient changes sign in Fig. 1.

The scope for a detailed comparison with the results in the previous section is limited, as the non-trace helium impurity strongly affects the transport of carbon in this LHD simulation, and the W7-X case of the previous section corresponds to a different magnetic

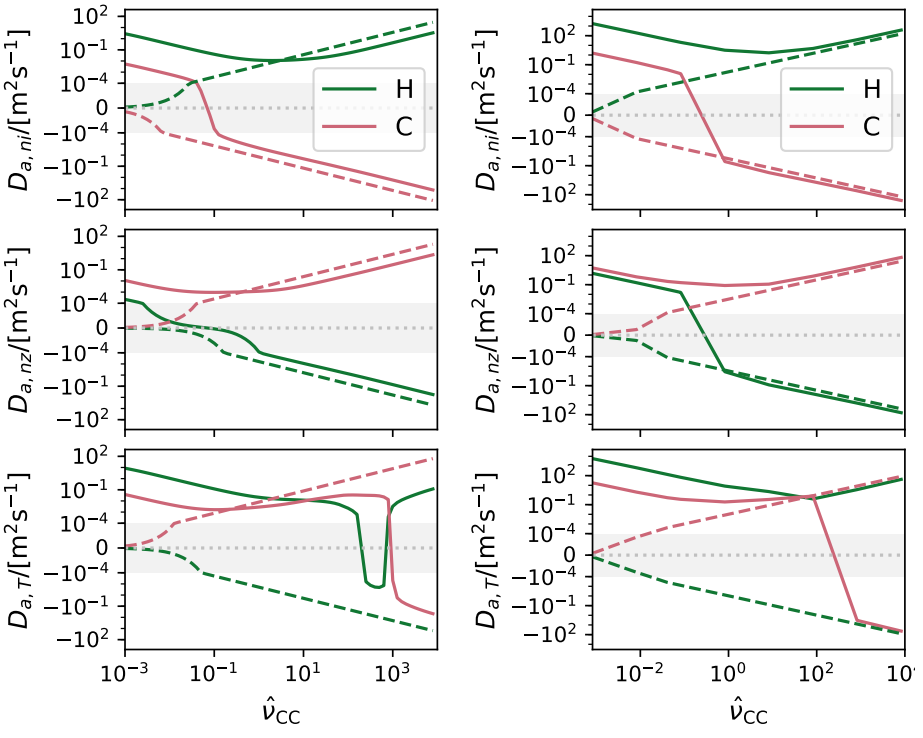

Figure 1: The neoclassical (—) and classical (- - -) transport coefficients as defined in (3.1), plotted against the impurity-impurity collisionality. Left column: W7-X standard case. Right column: LHD impurity-hole case. The classical coefficients were calculated using (2.9), while the neoclassical coefficients were calculated using SFINCS.

configuration. Nevertheless, the classical fluxes are comparable to the neoclassical fluxes, and clearly cannot be neglected in an analysis of the collisional transport.

Based on this conclusion, we have implemented the classical fluxes (2.9)-(2.10) as a post-processing step to the neoclassical codes SFINCS and DKES, see the supplementary material for an example implementation in python.

As a final remark, we note that since the neoclassical transport in W7-X is sufficiently low to be comparable to the classical, the transport due to micro-turbulence can become relatively more important. It may thus be necessary to consider the effect of turbulence on stellarator impurity transport in the future, which is often neglected due to the computational expense of simulating turbulence in stellarator geometry. Recent experimental studies by Langenberg *et al.* (2018) and Geiger *et al.* (2019) already point strongly in that direction.

SB and IP were supported by the International Career Grant of Vetenskapsrådet (Dnr. 330-2014-6313) and IP by Marie Sklodowska Curie Actions, Cofund, Project INCA 600398. SB's visit to Greifswald was supported by Chalmersska forskningsfonden. This work has been carried out within the framework of the EUROfusion Consortium and has received funding from the Euratom research and training programme 2014-2018 and 2019-2020 under grant agreement No 633053. The views and opinions expressed herein do not necessarily reflect those of the European Commission.

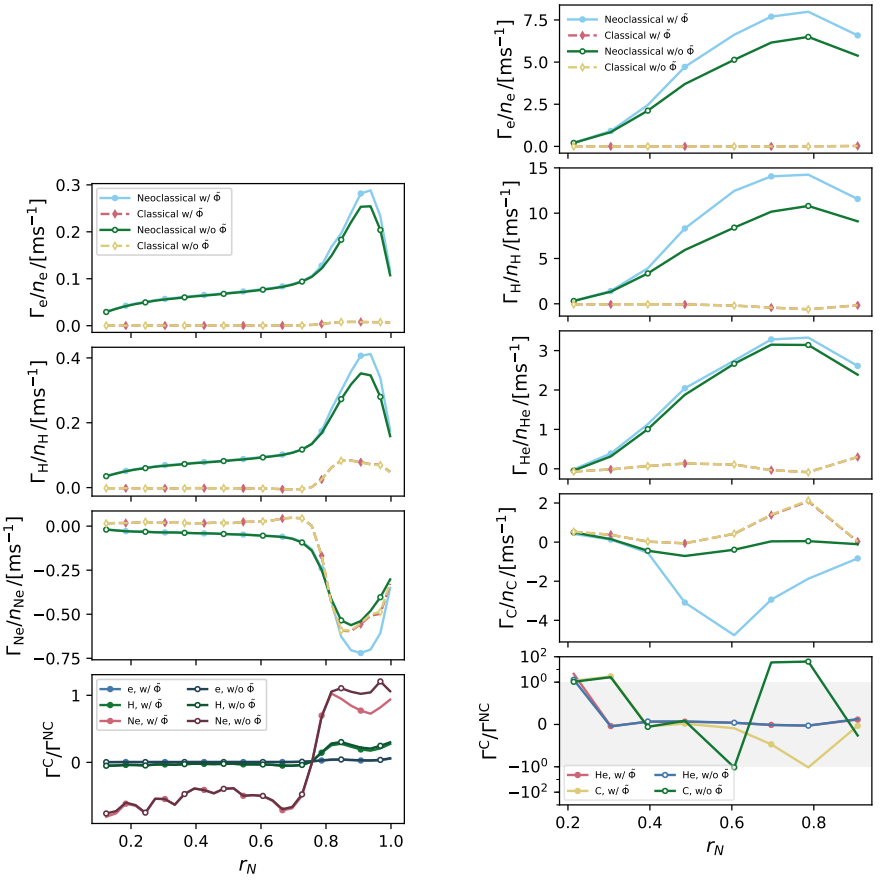

Figure 2: Neoclassical (—) and classical (---) fluxes for different species in W7-X (left) and LHD (right) as a function of normalized radius r_N. Filled (open) symbols show the flux with (without) the effect of $\tilde{\Phi}$ included. The lowest panels show the ratio of the classical and neoclassical transport.

Appendix A. Braginskii matrix elements

The Braginskii matrix elements are defined by

$$M_{ab}^{jk} = \frac{\tau_{ab}}{n_a} \int v_2 L_j^{(3/2)}(x_a^2) C_{ab} \left[\frac{m_a v_2}{T_a} L_k^{(3/2)}(x_a^2) f_{a0}, f_{b0} \right], \tag{A 1}$$

$$N_{ab}^{jk} = \frac{\tau_{ab}}{n_a} \int v_2 L_j^{(3/2)}(x_a^2) C_{ab} \left[f_{a0}, \frac{m_b v_2}{T_b} L_k^{(3/2)}(x_b^2) f_{b0} \right], \tag{A 2}$$

where v_2 is any Cartesian velocity component, f_{a0} is a Maxwellian, $x_a = v/\sqrt{2T_a/m_a}$, $L_k^{(3/2)}$ are Sonine polynomials, where the polynomials relevant to classical particle and heat transport are

$$L_0^{(3/2)}(x_a^2) = 1, \tag{A 3}$$

$$L_1^{(3/2)}(x_a^2) = \frac{5}{2} - x_a^2. \tag{A 4}$$

The corresponding relevant matrix elements are

$$M_{ab}^{00} = -\frac{\left(1+\frac{m_a}{m_b}\right)\left(1+\frac{m_a T_b}{m_b T_a}\right)}{\left(1+\frac{m_a T_b}{m_b T_a}\right)^{5/2}}, \tag{A 5}$$

$$M_{ab}^{01} = -\frac{3}{2}\frac{1+\frac{m_a}{m_b}}{\left(1+\frac{m_a T_b}{m_b T_a}\right)^{5/2}}, \tag{A 6}$$

$$M_{ab}^{11} = -\frac{\frac{13}{4}+4\frac{m_a T_b}{m_b T_a}+\frac{15}{2}\left(\frac{m_a T_b}{m_b T_a}\right)^2}{\left(1+\frac{m_a T_b}{m_b T_a}\right)^{5/2}}, \tag{A 7}$$

$$N_{ab}^{11} = \frac{27}{4}\frac{\frac{m_a}{m_b}}{\left(1+\frac{m_a T_b}{m_b T_a}\right)^{5/2}}. \tag{A 8}$$

(A 9)

REFERENCES

Beidler, C., Brakel, R., Burhenn, R., Dinklage, A., Erckmann, V., Feng, Y., Geiger, J., Hartmann, D., Hirsch, M., Jaenicke, R., Koenig, R., Laqua, H., Maassberg, H., Wagner, F., Weller, A. & Wobig, H. 2012 Fusion physics. chap. 8.3.6. Vienna: International Atomic Energy Agency.

Bolt, H., Barabash, V., Federici, G., Linke, J., Loarte, A., Roth, J. & Sato, K. 2002 Plasma facing and high heat flux materials needs for ITER and beyond. *Journal of Nuclear Materials* **307-311**, 43 – 52.

Braginskii, S. 1958 Transport phenomena in a completely ionized two-temperature plasma. *Sov. Phys. JETP* **6** (33), 358–369.

Braun, S. & Helander, P. 2010 Pfirsch-Schlüter impurity transport in stellarators. *Physics of Plasmas* **17** (7), 072514.

Buller, S., Smith, H. M., Helander, P., Mollén, A., Newton, S. L. & Pusztai, I. 2018 Collisional transport of impurities with flux-surface varying density in stellarators. *Journal of Plasma Physics* **84** (4), 905840409.

García-Regaña, J., Beidler, C., Kleiber, R., Helander, P., Mollén, A., Alonso, J., Landreman, M., Maassberg, H., Smith, H., Turkin, Y. & Velasco, J. 2017 Electrostatic potential variation on the flux surface and its impact on impurity transport. *Nuclear Fusion* **57** (5), 056004.

Geiger, B., Wegner, T., Beidler, C., Burhenn, R., Buttenschön, B., Dux, R., Langenberg, A., Pablant, N., Pütterich, T., Turkin, Y., Windisch, T., Winters, V., Beurskens, M., Biedermann, C., Brunner, K., Cseh, G., Damm, H., Effenberg, F., Fuchert, G., Grulke, O., Harris, J., Killer, C., Knauer, J., Kocsis, G., Krämer-Flecken, A., Kremeyer, T., Krychowiak, M., Marchuk, O., Nicolai, D., Rahbarnia, K., Satheeswaran, G., Schilling, J., Schmitz, O., Schröder, T., Szepesi, T., Thomsen, H., Mora, H. T., Traverso, P., Zhang, D. & The W7-X Team 2019 Observation of anomalous impurity transport during low-density experiments in W7-X with laser blow-off injections of iron. *Nuclear Fusion* **59** (4), 046009.

Hazeltine, R. D. 1973 Recursive derivation of drift-kinetic equation. *Plasma Physics* **15** (1), 77.

Helander, P., Newton, S. L., Mollén, A. & Smith, H. M. 2017 Impurity transport in a mixed-collisionality stellarator plasma. *Phys. Rev. Lett.* **118**, 155002.

Helander, P. & Sigmar, D. J. 2005 *Collisional Transport in Magnetized Plasmas*. Cambridge University Press.

Hinton, F. L. & Wong, S. K. 1985 Neoclassical ion transport in rotating axisymmetric plasmas. *The Physics of Fluids* **28** (10), 3082–3098.

Landreman, M., Smith, H. M., Mollén, A. & Helander, P. 2014 Comparison of particle trajectories and collision operators for collisional transport in nonaxisymmetric plasmas. *Physics of Plasmas* **21** (4), 042503.

Langenberg, A., Warmer, F., Fuchert, G., Marchuk, O., Dinklage, A., Wegner, T., Alonso, J. A., Bozhenkov, S., Brunner, K. J., Burhenn, R., Buttenschn, B., Drews, P., Geiger, B., Grulke, O., Hirsch, M., Höfel, U., Hollfeld, K. P., Killer, C., Knauer, J., Krings, T., Kunkel, F., Neuner, U., Offermanns, G., Pablant, N. A., Pasch, E., Rahbarnia, K., Satheeswaran, G., Schilling, J., Schweer, B., Thomsen, H., Traverso, P., Wolf, R. C. & the W7-X Team 2018 Impurity transport studies at Wendelstein 7-X by means of x-ray imaging spectrometer measurements. *Plasma Physics and Controlled Fusion* **61** (1), 014030.

Mollén, A., Landreman, M., Smith, H. M., Braun, S. & Helander, P. 2015 Impurities in a non-axisymmetric plasma: Transport and effect on bootstrap current. *Physics of Plasmas* **22** (11), 112508.

Mollén, A., Landreman, M., Smith, H. M., García-Regaña, J. M. & Nunami, M. 2018 Flux-surface variations of the electrostatic potential in stellarators: impact on the radial electric field and neoclassical impurity transport. *Plasma Physics and Controlled Fusion* **60** (8), 084001.

Newton, S. & Helander, P. 2006 Neoclassical momentum transport in an impure rotating tokamak plasma. *Physics of Plasmas* **13** (1), 012505.

Newton, S. L., Helander, P., Mollén, A. & Smith, H. M. 2017 Impurity transport and bulk ion flow in a mixed collisionality stellarator plasma. *Journal of Plasma Physics* **83** (5), 905830505.

Nührenberg, J. & Zille, R. 1986 Stable stellarators with medium β and aspect ratio. *Physics Letters A* **114** (3), 129 – 132.

Pfirsch, D. & Schlüter, A. 1962 Der einfluss der elektrischen leitfähigkeit auf das gleichgewichtsverhalten von plasmen niedrigen drucks in stelleratoren. *Max-Planck-Institut Report MPI/PA/7/62* pp. 88–89.